Scientific Research Publishing

World Journal of Mechanics, 2025, 15(4), 53-76
https://www.scirp.org/journal/wjm
ISSN Online: 2160-0503
ISSN Print: 2160-049X

Analysis of Deep to Moderately Deep Beams Using Timoshenko Theory and 2D Plane-Stress Elasticity

Christopher G. Provatidis

School of Mechanical Engineering, National Technical University of Athens, Athens, Greece
Email: cprovat@central.ntua.gr

How to cite this paper: Provatidis, C.G. (2025) Analysis of Deep to Moderately Deep Beams Using Timoshenko Theory and 2D Plane-Stress Elasticity. *World Journal of Mechanics*, **15**, 53-76.
https://doi.org/10.4236/wjm.2025.154004

Received: March 15, 2025
Accepted: April 27, 2025
Published: April 30, 2025

Abstract

This study examines rectangular cantilever beams, clamped at one end and subjected to a transverse tip load at the other, with aspect ratios $L/h = 1 \div 5$, a range in which shear deformation and stress field nonuniformities have a pronounced influence on structural behavior. A plane-stress finite element formulation is employed to capture the full two-dimensional elastic response, and the results are systematically compared with closed-form solutions derived from Timoshenko beam theory. The comparison highlights the limitations of classical beam assumptions within this aspect ratio range. Based on numerical evidence, approximate expressions for the maximum deflection under end loading are proposed for selected values of Poisson's ratio, offering improved accuracy for moderately deep and deep beams. In addition, a MATLAB® code is provided for estimating the maximum deflection for arbitrary values of Poisson's ratio.

Keywords

Timoshenko Beam, Transverse Displacement, Maximum Deflection, Static Analysis, Finite Elements

1. Introduction

A Google Scholar search for the term "Timoshenko beam" currently yields approximately 127,000 results—an increase of 1.6 times compared to the 78,000 entries reported in 2019 by Elishakoff [1].

Although much of the early research on the Timoshenko beam theory focused on vibrations [2] [3] and beams on elastic foundations [4], a substantial body of work has since addressed static analysis, including displacement and stress fields,

as documented in a recent monograph [5]. According to Conway *et al.* [6], the analysis of deep beams can be broadly classified into three categories: 1) infinite span with periodic loading, 2) infinite span with non-periodic loading, and 3) spans of finite length. In most cases, the Airy stress function is expressed as an infinite series of hyperbolic functions or Fourier integrals. Alternatively, the principle of the least work applied to the strain energy functional is sometimes employed [6] [7]. Using the Schwarz-Christoffel transformation, Theocaris [8] derived an analytical solution for the stress distribution in a semi-infinite strip subjected to a concentrated axial load, represented by a few terms of hyperbolic functions rather than an infinite series. The same author later extended the approach to cases involving distributed loads [9]. For the semi-infinite strip, Benthem [10] solved the clamped-end case by applying the Laplace transform to eliminate the longitudinal coordinate x from the differential equation governing the Airy stress function.

In the context of mixed boundary-value problems, Horvay and Born [11] proposed solutions in the form of infinite series composed of exponential and trigonometric functions for a semi-infinite elastic strip. Their work addressed two specific cases: 1) a prescribed quadratic shear displacement with zero normal stress, and 2) a prescribed cubic normal displacement with zero shear stress. Expanding on this approach, Johnson and Little [12] employed a series expansion involving ten hyperbolic terms to address all possible combinations of prescribed stresses and/or displacements along the short edge of the strip. This includes the pure displacement case, commonly referred to as the displacement problem.

Shear coefficients—defined as the ratio of the average shear strain over a cross-section to the shear strain at the centroid—have been computed by Cowper [13] for various cross-sectional geometries, including the rectangular section. For rectangular beams, Labuschagne *et al.* [14] conducted a comparative study of linear beam theories, namely Euler-Bernoulli, Timoshenko, and two-dimensional elasticity theory. For the same cross-sectional type, Levinson [15] proposed a shear coefficient of (5/6), a value that falls within the commonly reported range of 0.822 to 0.870 found in the literature for rectangular cross sections.

The present paper was primarily motivated by the fact that, within the context of computational mechanics, the exact deflection and associated stresses in an end-loaded cantilever are widely used as a benchmark test. Nevertheless, a question that persists to this day concerns the exact value of the maximum transverse displacement (also referred to as deflection). More specifically, the commonly used closed-form expression proposed by Timoshenko and Goodier [16] assumes a linear distribution of the normal stress σ_x and a parabolic distribution of the shear stress τ_{xy}.

To prevent rigid-body motion, three kinematical constraints were imposed: two displacement components at the midpoint of the fixed end and the axial displacement slope at the same location. As a result, since the slope of the neutral axis is non-zero, this model allows for shear strain at the support. Consequently, the re-

sulting analytical expression for total deflection includes contributions from both bending and shear forces.

However, it is well known that this analytical solution is characterized by warping of the displacement field near the built-in end. Due to this effect, the support region will henceforth be referred to as the *fixed* section, where the quotation denotes the presence of warping (with displacement components: $U \neq 0$ and $V \neq 0$) rather than complete constraint. In contrast, for the case where the beam's short edge is *fully fixed* ($U = V = 0$), we adopt the term *clamped* beam in the present study.

According to the above explanations, the analytical solution given by Timoshenko and Goodier [16] does not exactly describe the example of a horizontally oriented cantilever beam in which the right vertical edge is fully constrained (clamped). For this reason, the boundary conditions necessary to match the exact solution must be followed; otherwise, the FEM numerical solution converges to a smaller value [17]. The latter issue will be thoroughly discussed in this paper.

Alternatively, Livesley [18] modifies Timoshenko and Goodier [16] as follows. In addition to the two zero displacement components at the middle of the "fixed" section, he also reduces the horizontal displacement component at the upper end. Then, he found that the lower end of the fixed section is also fixed. Note that this issue is also cited as Exercise-5 in [16] (p. 63). In his textbook, Livesley [18] (pp. 94-95) uses his formula as a reference to compare the quality of one-dimensional finite elements for the deep beam. But the question is how accurate the latter analytical formula is.

Readers may also refer to Roark's formulas, which state that the shear displacement, V_s, can be determined using standard methods such as the method of unit loads or Castigliano's theorem. This result, however, requires multiplication by a form factor F, which is 6/5 for a rectangular cross-section [19].

The purpose of this paper is to clarify the mechanics of Timoshenko's beam, focusing on the following issues:

1) To evaluate the accuracy of the calculated deflection obtained using the correcting factor $F = 6/5$ (as reported in Ref. [19]).

2) To investigate which of the established formulas provide lower or upper bounds for the finite element solution.

3) To propose a practical algorithm and accompanying computer code for calculating the maximum deflection of a clamped beam subjected to a tip load.

To enhance reader comprehension, and despite Professor Timoshenko's contributions to all three formulas investigated herein, we will refer to them distinctly as Roark's, Timoshenko's, and Livesley's formulas. A comprehensive discussion can be found in Section 5.

2. Energy Conservation

Let us consider a rectangular beam of height h in the y-direction while its length in the x-direction is L. This cantilever has a narrow rectangular cross section of

width b (not shown) bent by a force P applied at the end O (Figure 1).

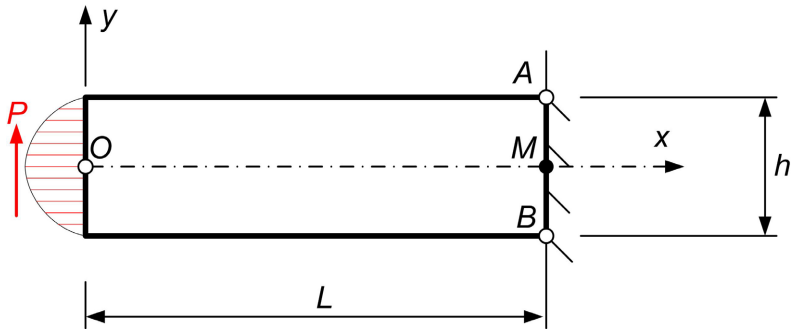

Figure 1. The cantilever Timoshenko's beam.

Following Timoshenko and Goodier [16], we adopt stress distribution according to Bernoulli theory, thus the normal stresses σ_x and σ_y follow the linear law:

$$\sigma_x = \frac{M}{I} y = -\frac{P}{I} xy \text{, and } \sigma_y = 0, \tag{1}$$

while the shear stress follows the well-known parabolic law:

$$\tau_{xy} = -\frac{6P}{bh^3}\left(\frac{h^2}{4} - y^2\right) = -\frac{P}{2I}\left(\frac{h^2}{4} - y^2\right). \tag{2}$$

The abovementioned second moment of inertia of the cross section is given by:

$$I = \frac{bh^3}{12}. \tag{3}$$

In general, the sign in the normal stress σ_x is positive when tension occurs. The lateral force P is taken upwards (*i.e.*, in the positive direction of y -axis), thus the upper fibers ($y > 0$) are in compression ($\sigma_x < 0$). Therefore, since the associated y coordinate of these fibers is positive ($y = +h/2$) a minus sign becomes necessary to be set in Equation (1). Moreover, the usual convention of positive shear stress τ_{xy} dictates a negative sign in Equation (2) as well.

The strain energy of the rectangular sheet (of dimensions $L \times b \times h$) is estimated by the volume integral of the strain energy density:

$$W = \frac{1}{2}\int_V \left(\sigma_x \varepsilon_x + \sigma_y \varepsilon_y + \tau_{xy}\gamma_{xy}\right) dV = \frac{1}{2}\int_V \left(\sigma_x \varepsilon_x + \tau_{xy}\gamma_{xy}\right) dxdydz \tag{4}$$

To determine the strain ε_x involved in Equation (4), we must consider the material constitutive law for the *plane-stress* state,

$$\begin{Bmatrix} \sigma_x \\ \sigma_y \\ \tau_{xy} \end{Bmatrix} = \frac{E}{1-\nu^2} \begin{bmatrix} 1 & \nu & 0 \\ \nu & 1 & 0 \\ 0 & 0 & \dfrac{(1-\nu)}{2} \end{bmatrix} \begin{Bmatrix} \varepsilon_x \\ \varepsilon_y \\ \gamma_{xy} \end{Bmatrix}. \tag{5}$$

According to Equation (1), we have $\sigma_y = 0$, thus eventually Equation (5) gives:

$$\sigma_x = E\varepsilon_x, \text{ and } \tau_{xy} = G\gamma_{xy}. \tag{6}$$

Taking the variables in the intervals $0 \le x \le L$, $-h/2 \le y \le h/2$, and $0 \le z \le b$, and substituting Equations (1), (2) and (6) into Equation (4), the strain energy splits in two volume integrals which can be analytically written as follows:

$$W_b = \frac{1}{2E}\int_V \sigma_x^2\, dxdydz = \frac{1}{2}\left(\frac{P^2}{E}\frac{4L^3}{bh^3}\right) = \frac{1}{2}\left(\frac{P^2L^3}{3EI}\right) \tag{7}$$

$$W_s = \frac{1}{2G}\int_V \tau_{xy}^2\, dxdydz = \frac{1}{2}\frac{P^2L}{(hb)G}\left[\frac{6}{5}\right] \tag{8}$$

Obviously, the total strain energy $W = W_b + W_s$ due to bending and shear components, must be equal to the external work of the shear force P plus the work W_{support} done by the reaction stresses at the supporting boundary ("fixed" section), thus we have:

$$\frac{1}{2}PV_o + W_{\text{support}} = \frac{1}{2}\left(\frac{P^2L^3}{3EI}\right) + \frac{1}{2}\frac{P^2L}{(hb)G}\left[\frac{6}{5}\right]. \tag{9}$$

For the rectangular sheet under study, the obtained factor $F = 6/5$ in Equation (9) is a standard for a cantilever beam. It has been widely written that it comes from the parabolic profile of the shear stress described by Equation (2).

In more details, the well-known *Shear Correction Factor* (SCF) k_s is defined as a factor that when applied to the actual cross-sectional area A produces an artificial area $A_s = k_s A$ associated with a virtual constant shear stress $\tau'_{xy} = P/A_s$ which yields the same strain energy as the actual strain distribution. For a rectangle in which the actual strain distribution is parabolic, *i.e.*, $\tau_{xy} = 6P/(bh^3)\left(h^2/4 - y^2\right)$, it is trivial to validate that $k_s = 5/6$ (see, e.g., [5]). Therefore, by replacing the actual cross-sectional area ($A = bh$) with the equivalent area $A_s = k_s A$, the inverse $F = 1/k_s = 6/5$ suddenly appears as a factor in front of the classical shear deflection $PL/(AG)$ if the whole rectangular beam is considered as a sole elastic element. To be more accurate, the latter occurs for every slice of dimensions "thickness × height" = $\Delta x \times h$, but thanks to the constant value of shear force $Q = P$ to every uniform cross section, we can apply the factor F to the average shear $\tau = P/A_s = G\gamma = G\left(V_s/L\right)$. Thus, solving the latter equation for V_s, we have:

$$V_s = \frac{PL}{A_s G} = \frac{PL}{(k_s A)G} = \frac{1}{k_s}\left(\frac{PL}{AG}\right) = F\left(\frac{PL}{AG}\right) \tag{10}$$

Equation (10), which was derived from scratch, is also suggested by Roark's formulas [12].

One may observe that the last term on the right-hand side of Equation (9), which is the shear work W_s of Equation (8), refers to the abovementioned work $\frac{1}{2}PV_s$. However, due to the still *unknown* work W_{support} in the left-hand side, we cannot yet solve Equation (9) in the total deflection V_0. Nevertheless, if we neglect the work W_{support} done by the reaction stresses at the supporting boundary, solving Equation (9) for the maximum deflection V_0, we receive the well-accepted approximation:

Roark's formula: $$\boxed{(V_o)_{\text{approx}} \approx \frac{PL^3}{3EI} + \frac{PL}{(hb)G}\left[\frac{6}{5}\right]}. \quad (11)$$

In other words, the maximum approximate deflection $(V_o)_{\text{approx}}$ in Equation (11) consists of the classical Bernoulli solution $V_b = PL^3/(3EI)$ plus the shear term:

$$V_s = \frac{PL}{(hb)G}\left[\frac{6}{5}\right]. \quad (12)$$

Again, Equation (12)—which was obtained here from scratch—coincides with that proposed by *Roark's formulas* [19].

On the other hand, Timoshenko and Goodier (see, [16] Eq. (r), p. 39) promote a larger shear value according to the formula:

$$V_s' = \frac{P(h^2/4)L}{2IG} = \frac{PL}{(bh)G}\left[\frac{3}{2}\right]. \quad (13)$$

Comparing Equation (12) with Equation (13), one may observe that the calculated shear deflections are quite different ($V_s < V_s'$) unless the shear modulus G in Timoshenko and Goodier's formula, expressed by Equation (13), is technically replaced by:

$$G_s = \frac{5}{4}G = 1.25G. \quad (14)$$

The reason for the discrepancy between Equations (12) and (13) is that the boundary conditions imposed in [16] lead to relatively large warping, and thus the associated mechanical work, W_{support}, *cannot* be neglected.

3. Analytical Solutions

To calculate the mechanical work W_{support} done by the reaction stresses at the supporting "fixed" boundary, we need to determine the displacement field in the beam and particularly along the "fixed" section AMB (see **Figure 1**).

3.1. Displacement Field

First, it is simple to verify that the stresses of Equations (1) and (2) satisfy the well-known equilibrium conditions:

$$\frac{\partial \sigma_x}{\partial x} + \frac{\partial \tau_{xy}}{\partial y} = 0, \text{ and } \frac{\partial \tau_{xy}}{\partial x} + \frac{\partial \sigma_y}{\partial y} = 0. \quad (15)$$

Considering the material constitutive law given by Equation (5), the stress equilibrium equations are converted into the so-called *Navier-Kirchhoff* equations in terms of only the displacement components:

$$\begin{aligned} &\frac{\partial^2 U}{\partial x^2} + \frac{1-\nu}{2}\frac{\partial^2 U}{\partial y^2} + \frac{1+\nu}{2}\frac{\partial^2 V}{\partial x \partial y} = 0, \\ &\frac{\partial^2 V}{\partial y^2} + \frac{1-\nu}{2}\frac{\partial^2 V}{\partial x^2} + \frac{1+\nu}{2}\frac{\partial^2 U}{\partial x \partial y} = 0. \end{aligned} \quad (16)$$

Integrating the Navier-Kirchhoff Equation (16) gives the general solution:

$$\mathbf{u}=\begin{Bmatrix}U(x,y)\\V(x,y)\end{Bmatrix}=\frac{P}{EI}\begin{Bmatrix}x^2y/2-y^3(2+\nu)/6-C_1y+C_2\\-\nu xy^2/2-x^3/6+\left[h^2(1+\nu)/4+C_1\right]x+C_3\end{Bmatrix}, \tag{17}$$

with C_1, C_2 and C_3 being constants of integration. Note that since the boundary conditions of this problem are of Neumann-type (prescribed tractions), the solution is not unique unless we prevent *rigid-body* motion. But even so, the solution for the displacement field (not the stresses) depends on the selected points at which boundary conditions of Dirichlet type are imposed. In an analogous way, prescribed flux in a closed domain governed by Laplace/Poisson equation does not ensure a unique solution unless the potential is prescribed at least to one boundary point. Again, now that the problem is plane stress elasticity, we need the restriction of three degrees of freedom to prevent rigid-body motion of the rectangular beam. This constraint can be realized in various ways, which however lead to different displacement fields and thus to *different* warping patterns. Below, we shall study two typical cases.

3.1.1. Case-1: Timoshenko and Goodier [16]

To prevent the abovementioned rigid-body motion, Timoshenko and Goodier [16] impose zero displacement components at the middle point M ($U_M=V_M=0$) of the fixed section as shown in **Figure 1**, and hence we have $C_2=0$ and $C_3=L^3/6-\left[h^2(1+\nu)/4+C_1\right]L$. In addition, they also fix a vertical segment of the cross-section at the same point M ($x=L, y=0$). Hence, this particular condition $(\partial U/\partial x)_{x=L,y=0}=0$, leads to $C_1=L^2/2$, so $C_3=-L^3/3-h^2L(1+\nu)/4$. The results are also shown in the first line of **Table 1**.

Table 1. Constants for the prevention of rigid-body motion.

Author	Boundary conditions	C_1	C_2	C_3
Timoshenko and Goodier [16]	$U_M=0$, $V_M=0$, $(\partial U/\partial x)_M=0$	$\frac{L^2}{2}$	0	$-\frac{L^3}{6}-\frac{(1+\nu)h^2L}{4}$
Livesley [18]	$U_M=0$, $V_M=0$, $U_A=0$	$-\frac{L^2}{2}-\frac{(2+\nu)h^2}{24}$	0	$-\frac{L^3}{6}-\frac{(4+5\nu)h^2L}{24}$

Remark: It should become clear that Timoshenko and Goodier [16] eventually applied the condition $(\partial U/\partial x)_{x=L,\,y=0}=0$. Before that, they showed that the alternative condition $(\partial V/\partial x)_{x=L,\,y=0}=0$ leads to the well-known value $PL^3/(3EI)$ (Bernoulli solution), usually derived in elementary books on the strength of materials.

Based on the constants shown in the second row of **Table 1** (labelled as Timoshenko and Goodier [16]), Equation (17) gives the following displacements (note that the subscript "T" stands for Timoshenko):

Maximum deflection:

$$V_T(0,0)=\frac{PL^3}{3EI}\left[1+3(1+\nu)\frac{h^2}{4L^2}\right], \tag{18}$$

which may also be written as:

$$V_T(0,0)=\frac{PL^3}{3EI}+\frac{P(h/2)^2 L}{2GI}=\frac{PL^3}{3EI}+\frac{3PL(1+\nu)}{Ebh}. \tag{19}$$

Displacement component at "fixed" section in x-direction:

$$U_T(L,y)=\frac{(2+\nu)P}{6EI}y^3. \tag{20}$$

Displacement component at "fixed" section in y-direction:

$$V_T(L,y)=\frac{\nu PL}{2EI}y^2. \tag{21}$$

3.1.2. Case-2: According to Livesley [18]

Following Livesley [18] (p. 95), the boundary conditions are modified as follows. The point M ($x=L, y=0$) in the middle of support section AB is fully fixed and the upper point A of the same section (see Figure 1) is restrained to move horizontally, thus we have:

1) Point M: $U=V=0$ at $(x=L, y=0)$, and

2) Point A: $U=0$ at

$$(x=L, y=h/2). \tag{22}$$

These conditions determine the arbitrary constants in Equation (17) as follows: $C_1=L^2/2-(2+\nu)h^2/24, C_2=0, C_3=-L^3/3-h^2 L(4+5\nu)/24$, eventually giving:

$$\mathbf{u}\triangleq\begin{Bmatrix}U(x,y)\\V(x,y)\end{Bmatrix}=\left(\frac{P}{2EI}\right)\begin{Bmatrix}y\left(x^2-L^2\right)+\frac{1}{3}(2+\nu)y\left(\frac{h^2}{4}-y^2\right)\\\left(L^3-x^3\right)/3+\left[L^2+h^2(4+5\nu)/12\right](x-L)-\nu xy^2\end{Bmatrix} \tag{23}$$

Note that, because of symmetry, U is also zero at the lower point B $(x=L, y=-h/2)$ shown in Figure 1. Thus, the condition $U=0$ applies to both extreme points A and B at $y=\pm h/2$.

The vertical displacement of the tip O of the cantilever is given by

$$V_L(0,0)=\left(\frac{PL^3}{3EI}\right)\left[1+(2+2.5\nu)\frac{h^2}{4L^2}\right]=\left(\frac{PL^3}{3EI}\right)+\frac{(4+5\nu)PL}{2Ebh} \tag{24}$$

Moreover, regarding the warping along the fixed edge, the useful formulas are given by

x-direction: $U_L(L,y)=-\frac{(2+\nu)P}{6EI}y\left(\frac{h^2}{4}-y^2\right)$ (25)

y-direction: $V_L(L,y)=\frac{\nu PL}{2EI}y^2$ (26)

3.2. Comparison between the Two Cases

So far, we have seen that none of the above two cases, "T" and "L", ensures full fixation of the initially supposed "fixed" section but eventually found to be warped.

The warping profiles in the x-direction are compared in Figure 2 (points A, M, and B are the same as those illustrated in Figure 1 but rotated in clockwise direction by 90˚). There, one may observe that in Case 1 (Timoshenko and Goodier: Equations (18)-(21)), the warping vanishes only at the middle point M and is opposite to the existing tension and compression associated with parts MB and MA, respectively (clockwise reaction moment). In contrast, in Case 2 (Livesley: Equations (24)-(26)), the warping is more reasonable (vanishes at three points, A, M and B) but is consistent to the dominating tension and compression (anticlockwise reaction moment). In both cases, Equations (20) and (25) suggest that, although the expressions are *different*, the variation of the longitudinal $U(y)$-displacement with respect to the offset y is *cubic* ($U \propto y^3$) on the clamp.

Regarding the warping profiles in the y-direction, Equation (21) coincides with Equation (26), and thus in both cases we receive *identical* vertical (transverse) displacements ($V(y)$) of *quadratic* shape ($V \propto y^2$) on the clamp.

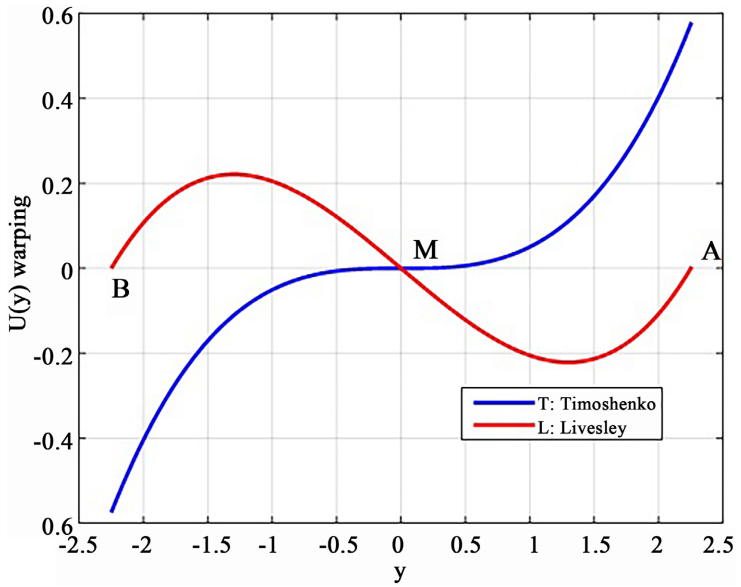

Figure 2. Warping of the "fixed" section according to Timoshenko and Goodier [16] and Livesley [18] modes $(E=1, \nu=0.30, L=9, h=4.5, b=1, P=1)$.

4. Work associated with the Warping

Below, we provide analytical formulas in both cases, "T" and "L" (defined in Section 3).

4.1. Timoshenko and Goodier Formula [16] ("T")

The warped section at ($x=L$) is described by the displacement components U_T

and V_T, which are described by Equations (20) and (21). The work done to create this warping is made by the stresses σ_x and τ_{xy}, which are associated with the displacements $U_T(L,y)$ and $V_T(L,y)$, respectively. The stresses are given by Equation (1) and Equation (2).

Due to the symmetric profile of stress and displacement with respect to the middle point M, in both directions the work along the entire "fixed" section AMB is double of the work along the half-side MA. Therefore, considering that the subscript "b" stands for bending whereas "s" for shear, we have:

$$\begin{aligned}\left(W_{AMB}\right)_{T,b} &= 2W_{MA}\\ &= 2\cdot\frac{1}{2}\int_0^{h/2}\sigma_x U_T(L,y)\,b\,dy\\ &= 2\cdot\frac{1}{2}\int_0^{h/2}\left(-\frac{PL}{I}y\right)\left[\frac{(2+\nu)P}{6EI}y^3\right]bdy\\ &= -\frac{1}{2}\cdot\frac{3P^2(2+\nu)L}{10Ebh}\end{aligned} \tag{27}$$

and

$$\begin{aligned}\left(W_{AMB}\right)_{T,s} &= 2\left(W_{MA}\right)_s\\ &= 2\cdot\frac{1}{2}\int_0^{h/2}\tau_{xy}V_T(L,y)bdy\\ &= 2\cdot\frac{1}{2}\int_0^{h/2}\left[-\frac{P}{2I}\left(h^2/4-y^2\right)\right]\left[\frac{\nu PL}{2EI}y^2\right]bdy\\ &= -\frac{1}{2}\cdot\frac{3P^2\nu L}{10Ebh}.\end{aligned} \tag{28}$$

The algebraic sum of the two above work components gives the total work for the linear and parabolic stresses (given by Equations (1) and (2), respectively) to create the warping, thus we have:

$$\begin{aligned}\left(W_{\text{support}}\right)_T &= \left(W_{AMB}\right)_{T,b}+\left(W_{AMB}\right)_{T,s}\\ &= -\frac{1}{2}\cdot\frac{3P^2L(1+\nu)}{5Ebh}\end{aligned} \tag{29}$$

The consideration of the above work $\left(W_{\text{support}}\right)_T$ leads to a change of the work done by the total external shear force P (of which an equivalent may be taken at the middle of the left edge) thus:

$$\frac{1}{2}P\left(\Delta V_o\right)_T = \left(W_{\text{support}}\right)_T \tag{30}$$

It is worthy to mention that if the above work $\left(W_{\text{support}}\right)_T$ is substituted in the approximate Equation (9), the produced result $V_T(0,0)$ becomes

$$\begin{aligned}V_T(0,0) &= \left(V_o\right)_{\text{approx}}-\left(\Delta V_o\right)_T\\ &= \left(\frac{P}{E}\cdot\frac{L^3}{3I}\right)+\frac{PL}{(hb)G}\left[\frac{6}{5}\right]+\frac{3PL(1+\nu)}{5Ebd}\end{aligned}$$

$$= \left(\frac{PL^3}{3EI} \right) + \frac{3PL(1+\nu)}{Ebh}, \tag{31}$$

Remark: Comparing Equation (31) with Equation (19), we see that after the above correction of Roark's formula [19] considering the warping work, we receive exactly the solution proposed by Timoshenko and Goodier [16].

4.2. Livesley's Formula [18] ("L")

In this subsection, we consider the displacement field according to the kinematical assumptions made by Livesley [18] (p. 95), in which the warping along the edge AMB is given according to Equations (25) and (26). In a similar way, due to the symmetric profile of stress σ_x and displacement $U(L,y)$ with respect to the middle M, the first work is double of the work along the half-side MA in the x-direction, and due to Equations (1) and (2) as well as Equations (25) and (26), we have ("b" = bending, "s" = shear):

$$\begin{aligned}
\left(W_{ABC}\right)_{L,b} &= 2\left(W_{AB}\right)_{L,b} \\
&= 2\cdot\frac{1}{2}\int_0^{h/2} \sigma_x U(L,y) b\, dy \\
&= 2\cdot\frac{1}{2}\int_0^{h/2} \left(-\frac{PL}{I}y\right)\left[-\frac{(2+\nu)P}{6EI}y\left(h^2/4-y^2\right)\right] b dy, \\
&= \frac{1}{2}\cdot\frac{P^2(2+\nu)Lbh^5}{720EI^2} \\
&= \frac{1}{2}\cdot\frac{P^2(2+\nu)L}{5Ebh}
\end{aligned} \tag{32}$$

The second work is also double the work along the half-side AB in the y-direction, thus

$$\begin{aligned}
\left(W_{AMB}\right)_{L,s} &= 2\left(W_{MA}\right)_{L,s} \\
&= 2\cdot\frac{1}{2}\int_0^{h/2} \tau_{xy} V(L,y) b dy \\
&= 2\cdot\frac{1}{2}\int_0^{h/2} \left[-\frac{P}{2I}\left(h^2/4-y^2\right)\right]\left[\frac{P}{2EI}\nu L y^2\right] b dy, \\
&= -\frac{1}{2}\cdot\frac{P^2\nu Lbh^5}{480EI^2} \\
&= -\frac{1}{2}\cdot\frac{3P^2\nu L}{10Ebh}.
\end{aligned} \tag{33}$$

As previously happened, the algebraic sum of the two above work components gives the total work for the linear and parabolic stresses (given by Equations (1) and (2), respectively) to create the warping, thus we have:

$$\begin{aligned}
\left(W_{\text{support}}\right)_L &= \left(W_{AMB}\right)_{L,b} + \left(W_{AMB}\right)_{L,s} \\
&= \frac{1}{2}\cdot\frac{P^2L(4-\nu)}{10Ebh}.
\end{aligned} \tag{34}$$

The consideration of the above work, $(W_{\text{support}})_L$, leads to a change of the work

done by the total external shear force P (of which an equivalent sum may be taken at the middle of the left edge) thus:

$$\frac{1}{2}P\left(\Delta V_o\right)_L = \left(W_{\text{support}}\right)_L \tag{35}$$

In a similar manner with Subsection 4.1, if $\left(W_{\text{support}}\right)_L$ is substituted in the approximate Equation (9), now the produced result $V_L(0,0)$ becomes

$$\begin{aligned} V_L(0,0) &= \left(V_o\right)_{\text{approx}} - \left(\Delta V_o\right)_L \\ &= \left(\frac{PL^3}{3EI}\right) + \frac{(4+5\nu)PL}{2Ebh}. \end{aligned} \tag{36}$$

As previously, comparing Equation (36) with Equation (26), we see that after the above correction we receive exactly the solution proposed by Livesley [18].

Remark: Comparing Equation (29) with Equation (34), one may observe that the two works done at the warped support are *different* each other. Obviously, their difference ΔW determines the difference ΔV between the deflections at the free end, through the equality $\frac{1}{2}P\Delta V = \Delta W$. This fact comes from the application of Equation (9) twice, the first time for the "T"-model and the second time for the "L"-model and then their subtraction by parts.

5. Deflection Bounds

From the above discussion, we have determined three possible formulas, as follows:

1) Roark's formula, given by Equation (11).

2) Timoshenko's formula, given by Equation (31).

3) Livesley's formula, given by Equation (36).

The classification of the beam depends on the *aspect ratio* (length: height), which is defined as follows:

$$\lambda = \frac{L}{h}. \tag{37}$$

Introducing the common coefficient:

$$\alpha = \frac{PL}{Ebh} = \frac{\lambda P}{Eb}, \tag{38}$$

the above estimations are proportional to λ and can be written as follows:

Roark's formula (Equation (11)):

$$\left(V_{\text{s, Roark}}\right)_{\max} = \frac{12}{5}(1+\nu)\alpha, \tag{39}$$

Timoshenko's formula (Equation (31)):

$$\left(V_{\text{s, Timoshenko}}\right)_{\max} = 3(1+\nu)\alpha, \tag{40}$$

Livesley's formula (Equation (36)):

$$\left(V_{\text{s, Livesley}}\right)_{\max} = \frac{4+5\nu}{2}\alpha, \tag{41}$$

Taking the first derivative of the above set with respect to λ, we obtain:

Roark's formula (Equation (11)):

$$\frac{d\left(V_{\mathrm{s,Roark}}\right)_{\max}}{d\lambda}=\frac{12}{5}(1+\nu)\left(\frac{P}{Eb}\right), \tag{42}$$

Timoshenko's formula (Equation (31)):

$$\frac{d\left(V_{\mathrm{s,Timoshenko}}\right)_{\max}}{d\lambda}=3(1+\nu)\left(\frac{P}{Eb}\right), \tag{43}$$

Livesley's formula (Equation (36)):

$$\frac{d\left(V_{\mathrm{s,Livesley}}\right)_{\max}}{d\lambda}=\frac{4+5\nu}{2}\left(\frac{P}{Eb}\right), \tag{44}$$

A first observation on Equations (39)-(41) is that for the same Poisson's ratio ν, for any two formulas out of the three, there is a corresponding linear relationship between the relevant shear deflection V_s, which is *independent* of the aspect ratio λ. For example, omitting the subscript "max", we have:

$$\frac{V_{\mathrm{s,Roark}}}{V_{\mathrm{s,Timoshenko}}}=\frac{4}{5}, \tag{45}$$

and

$$\frac{V_{\mathrm{s,Roark}}}{V_{\mathrm{s,Livesley}}}=\frac{24(1+\nu)}{5(4+5\nu)}. \tag{46}$$

Considering that Poisson's ratio varies within the interval $0.15\le\nu\le 0.30$ (from concrete to steel), the value predicted by Roark's formula (Equation(11) and Equation (39)) falls *between* those obtained using Timoshenko's and Livesley's boundary conditions (Equation (40) and Equation(41), respectively). Therefore, it is imperative to determine which of them provides the closest approximation to the converged finite element solution, that will be regarded as the most accurate reference.

The above observations are validated using a finite element (FEM) model of plane-stress elasticity (4-node bilinear rectangular elements), with $n_x=600$ uniform subdivisions in the longitudinal x-direction. The number of elements in the transverse y-direction, n_y, is chosen that all elements are square. The beam length is kept at a standard value (e.g., $L=3$), and its height $h=L/\lambda$ is continuously regulated accordingly, while all other quantities equal to unit $(b=1,E=1,P=1)$.

The abovementioned mesh density was selected because convergence was achieved at the fifth decimal place, which is sufficient for our purposes. For instance, in the case examined $(\lambda=1,\nu=0.15)$, a uniform mesh was progressively refined from 100 × 100 to 600 × 600 elements in increments of 100. The corresponding maximum deflections were found to be 6.67544, 6.67605, 6.67618, 6.67623, 6.67625, and 6.67626, respectively.

The arithmetic value of length L does not play any role at all, because—for prescribed values of load P, material properties (E,ν), and thickness b—the maximum deflection depends only on the aspect ratio λ, according the follow-

ing formulas:

$$V_{\text{Bernoulli}} = \frac{PL^3}{3EI} = \frac{4P}{Eb}\lambda^3, \tag{47}$$

where the shear component, second term of Roark's formula (Equation (11)), becomes:

$$V_s = \frac{PL}{(hb)G}\left[\frac{6}{5}\right] = \frac{12P(1+\nu)}{5Eb}\lambda. \tag{48}$$

For example, if Poisson's ratio is taken as $\nu = 0.30$, one may observe in Table 2 that for a broad spectrum of aspect ratios $\lambda = L/h$, the FEM-values, which are taken as a reference, lie between Livesley's model (*i.e.*, Equation (36)) and Roark's model (Equation (11)). In contrast, Timoshenko's formula (*i.e.*, Equation (31)) overestimates the maximum deflection. By subtracting the Bernoulli component, $V_{\text{Bernoulli}}$, the same results (in terms of only the shear displacement V_s) are shown in Figure 3.

Table 2. Total maximum deflection $V = V_{\text{Bernoulli}} + V_s$ (for $E = 1$, $\nu = 0.30$, $b = 1$, $P = 1$).

Model	$\lambda = 1.0$	$\lambda = 1.5$	$\lambda = 2.0$	$\lambda = 2.5$	$\lambda = 3.0$	$\lambda = 3.5$	$\lambda = 4.0$
Livesley	6.7500	17.6250	37.5000	69.3750	116.2500	181.1250	267.0000
FEM	6.9618	17.9159	37.8368	69.7246	116.5790	181.3996	267.1856
Roark	7.1200	18.1800	38.2400	70.3000	117.3600	182.4200	268.4800
Timoshenko	7.9000	19.3500	39.8000	72.2500	119.700	185.1500	271.6000

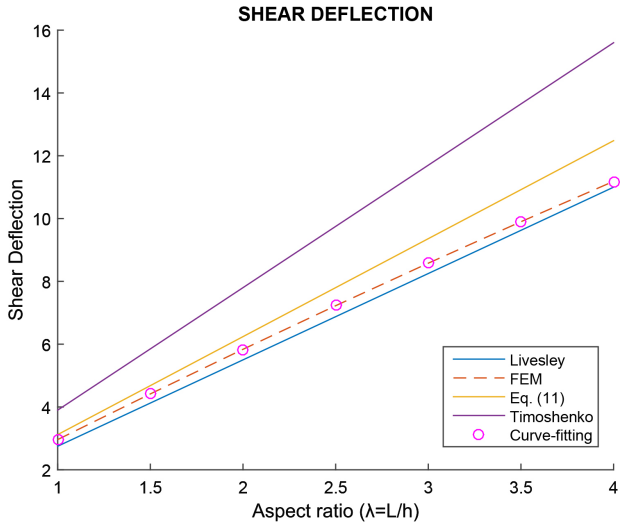

Figure 3. Shear deflection using all the four models ($\nu = 0.30$).

Overall, for a broader range of Poisson's ratios ($\nu = 0.15, 0.20, 0.25, 0.30$), the shear deflection V_s, coming from the FEM solution, is illustrated in Figure 4.

One may observe:

1) With adequate accuracy, the FEM solution can be represented by a straight line in the graph V_s versus λ. The slope of this line depends on Poisson's ratio ν, as also shown in Figure 5. One may observe that as Poisson's ratio increases

the shear deflection increases as well, and thus the corresponding line moves upwards.

2) For the smallest studied aspect ratio $\lambda = 1$, and any value of Poisson's ratio ν, the FEM-solution almost belongs to the Roark's curve, defined by Equation (11).

3) As Poisson's ratio ν increases, the FEM-curve tends to Livesley's curve, that is defined by Equation (36).

4) For Poisson's ratio $\nu = 0.30$ and the largest studied aspect ratio $\lambda = 5$, the FEM-solution almost belongs to Livesley's curve, defined by Equation (36).

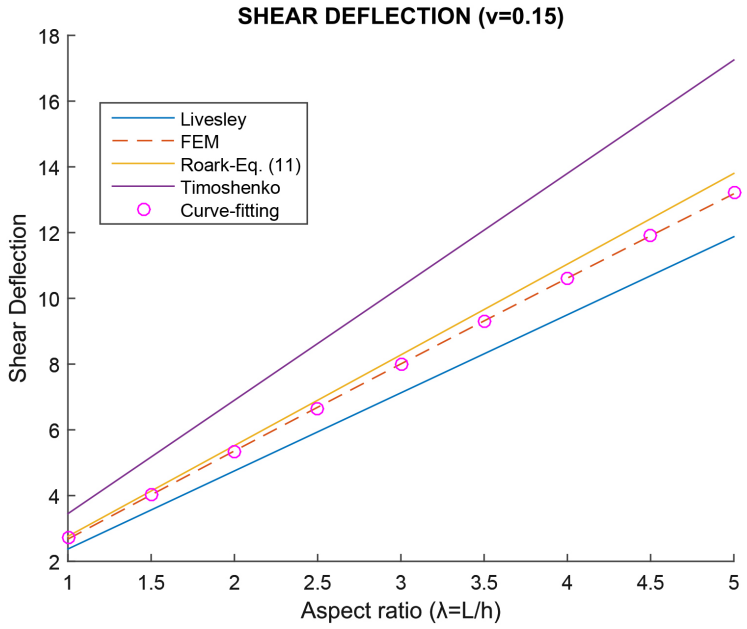

(a)

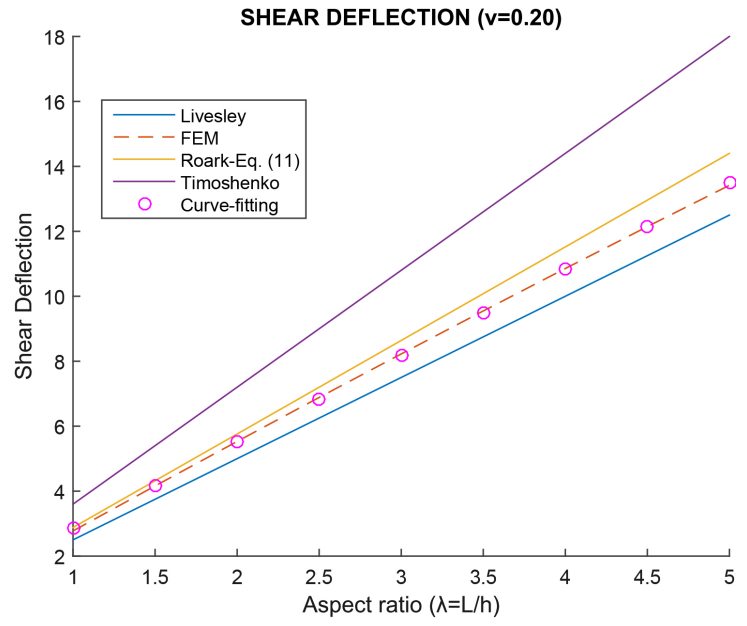

(b)

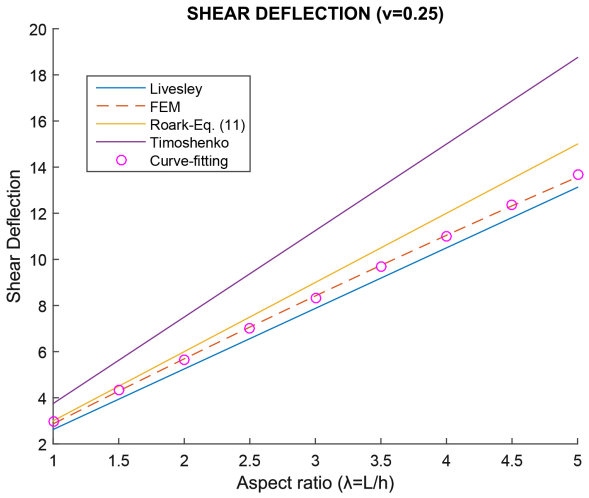

(c)

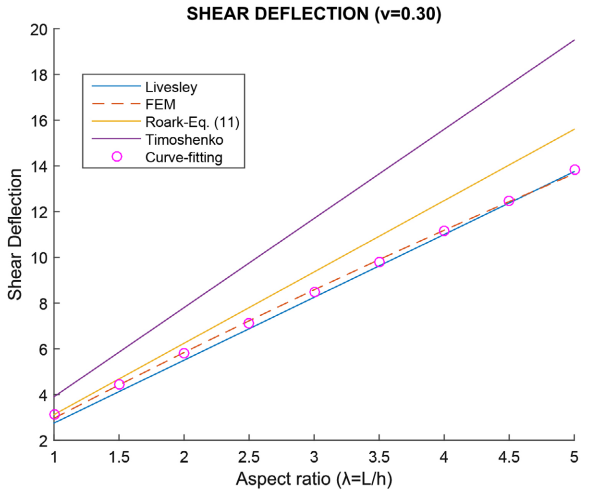

(d)

Figure 4. FEM calculations versus analytical models for several Poisson's ratios: (a) $\nu = 0.15$; (b) $\nu = 0.20$; (c) $\nu = 0.25$; (d) $\nu = 0.30$.

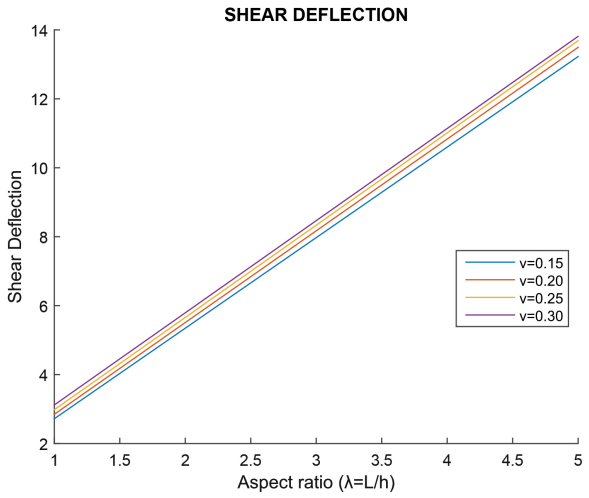

Figure 5. Shear deflection calculated using FEM, for several Poisson ratios (ν).

6. Curve Fitting

In the previous section, we showed that for each of the four Poisson's ratios $\nu \in [0.15, 0.30]$, we have determined one polygonal line that consists of nine points. Each of these nine points, is associated with one discrete aspect ratio, which varies in the interval $\lambda \in [1,5]$, with a constant step $\Delta\lambda = 0.5$. All the four curves (one for each Poisson's ratio) can be fitted in several manners, but in this paper, we present only two of them, as follows:

1) Linear interpolation. The regression formulas and the R-squared values are shown in Table 3.

2) Cubic interpolation (true cubic polynomial interpolation), with $R^2 = 1.0000000$, is shown in Table 4.

Table 3. Linear regression for the shear deflection V_s, based on FEM results ($E = 1$, $b = 1$, $P = 1$).

Poisson's ratio (ν)	Linear interpolation	R-squared
0.15	$0.0934210 + 2.6266105\,\lambda$	0.99993159
0.20	$0.1870982 + 2.6613086\,\lambda$	0.99981251
0.25	$0.3050623 + 2.6765495\,\lambda$	0.99957846
0.30	$0.4463497 + 2.6731285\,\lambda$	0.99916785

Table 4. Cubic regression formulas for the shear deflection V_s, based on FEM results ($E = 1$, $b = 1$, $P = 1$).

Poisson's ratio	Linear interpolation formula $V_s(\lambda)$
0.15	$-0.0377226 + 2.7291290\,\lambda - 0.0144925\,\lambda^2 - 0.0005197\,\lambda^3$
0.20	$-0.0388392 + 2.8411293\,\lambda - 0.0272371\,\lambda^2 - 0.0005475\,\lambda^3$
0.25	$-0.0399248 + 2.9533411\,\lambda - 0.0431638\,\lambda^2 - 0.0005946\,\lambda^3$
0.30	$-0.0409802 + 3.0657574\,\lambda - 0.0621308\,\lambda^2 - 0.0006626\,\lambda^3$

7. Interpolation Algorithms

Since the FEM solution was found to be bounded by Livesley's and Roark's curves, and because it monotonically rotates in the clockwise direction, for a given arbitrary pair (ν, λ), we can approximate the FEM solution by implementing one of the following algorithms (Sections 7.1 to 7.3).

7.1. Algorithm-1: Using Only the Endpoints and Linear Interpolations

This algorithm is as follows:

1) We perform linear interpolation between the four curves at $\lambda = 1$, and thus determine the value $(V_s)_{\text{left}}$ (denoted by "Left" on the blue line of Figure 6).

2) We perform linear interpolation between the four curves at $\lambda = 5$, and thus determine the value $(V_s)_{\text{right}}$ (denoted by "Right" on the red line of Figure 6).

3) Based on the above two values, $(V_s)_{\text{left}}$ and $(V_s)_{\text{right}}$, we linearly interpolate in terms of λ, and thus determine the desired value V_s.

In general, the *linear interpolation* between $(V_s)_{\text{left}}$ and $(V_s)_{\text{right}}$ leads to a small error. For example, if we pretend that the value V_s at ($\nu = 0.20$ and $\lambda = 3$) is unknown, the above procedure gives $(V_s)_{\text{interp}} = 8.0958$, while the FEM solution is $(V_s)_{\text{FEM}} = 8.2245$. Therefore, a more accurate procedure is under demand (see Sections 7.2 to 7.3).

7.2. Algorithm-2: Linear Interpolation Based on Local Data

An alternative procedure is to work as follows:

1) For the given λ-value, we perform *linear interpolation* and determine four values V_s on the corresponding polygonal curves of the FEM-results associated with four Poisson's ratios $\nu = 0.15$, 0.20, 0.25, and 0.30.

2) For the given ν-value, which is generally different than the above standardized ones, we perform a *linear interpolation* among the above four values V_s.

A MATLAB® code, which implements Algorithm-2, is given in **Appendix**. The reader may execute this code and will find the anticipated value $V_s = 8.2245$.

7.3. Algorithm-3: Higher Degree Interpolation

This is probably the most accurate algorithm of this section. A similar procedure with Algorithm-2 is applied, with the difference that—instead of the abovementioned linear interpolation (polygonal line by FEM results)—we perform cubic interpolation as follows:

1) For the given λ-value, we apply a *cubic* interpolation—according to **Table 4**—on each of the four cubic lines associated with four Poisson's ratios $\nu = 0.15$, 0.20, 0.25, 0.30. Therefore, four discrete values V_s are determined.

2) Having found the above four values on the interpolated curves, we then perform linear (or better *cubic* interpolation) between these four values.

The application of Algorithm-3 leads to the anticipated value $V_s = 8.2245$.

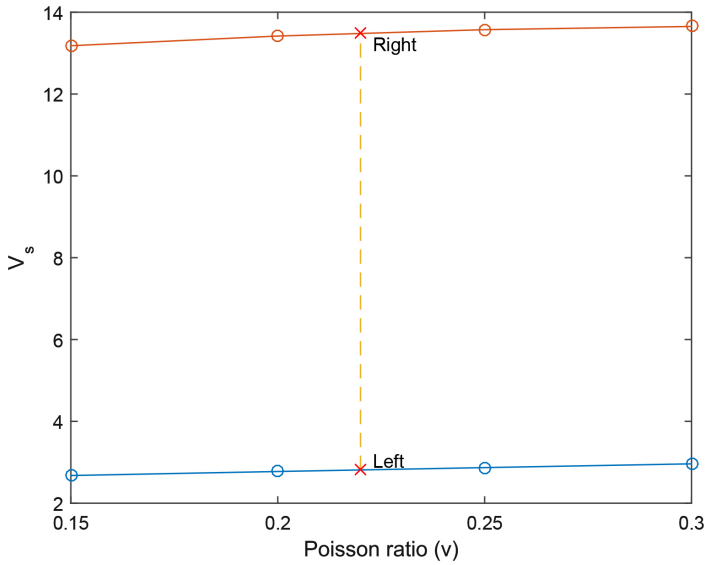

Figure 6. Left and right limits in terms of Poisson ratio (ν).

8. Discussion

The mechanical behavior of homogeneous beams mainly depends on the aspect ratio $\lambda = L/h$, where L is the length and h is the height. The standard definitions typically break down as follows:

1) $\lambda \le 2$: Deep beam—Requires 2D or 3D theory (not simple beam theory). Shear deformation is dominant; plane sections do *not* remain plane. 2D elasticity is needed to capture full stress state.

2) $2 \le \lambda \le 5 \div 10$: Timoshenko beam—First-order shear deformation theory. Both bending and shear are significant. Timoshenko or 2D plane stress gives good accuracy.

3) $\lambda \ge 10$: Euler-Bernoulli beam—Classical beam theory applies. Shear deformation is negligible; plane sections remain plane.

This study focused on the case of a clamped beam subjected to a transverse tip load, with an aspect ratio ranging from $1 \le L/h \le 5$. Over this entire range, the plane-stress model is applicable. We found that the calculated FEM curve (maximum deflection V_s versus aspect ratio λ) exhibits near-linear behavior and is bounded by the values proposed by Livesley [18] and Roark's formula [19], which serve as lower and upper limits, respectively. Conversely, a formula cited in the textbook by Timoshenko and Goodier [16] yields higher, thus conservative, values.

For discrete Poisson's ratios of $\nu = 0.15$, 0.20, 0.25, and 0.30, we performed linear and cubic regression analyses on the Finite Element Method (FEM) results. These regressions establish a relationship between the maximum shear deflection (V_s) and the continuous variable aspect ratio (λ). By incorporating the conventional Bernoulli bending term ($PL^3/(3EI)$), the total deflection can be readily determined.

Based on the four closed-form expressions of regression, we propose the following approach for an arbitrary Poisson's ratio $\bar{\nu}$: For a given aspect ratio $\lambda = L/h$, we utilize readily available cubic fitting formulas to determine the maximum shear deflection V_s for discrete Poisson's ratio values of $\nu = 0.15$, 0.20, 0.25, and 0.30. Subsequently, we merely interpolate for the specified Poisson's ratio $\bar{\nu}$.

On the Use of Plane-Strain for Low Aspect Ratios. While the present study adopts a plane-stress formulation suitable for aspect ratios between 1 and 5, structures with aspect ratios significantly less than 1 exhibit behavior that is no longer well-described by plane-stress assumptions. In such cases, one possible alternative is to employ a plane-strain model, which is appropriate when the structure extends uniformly in the out-of-plane direction and deformation is constrained along that axis—conditions typical in long prismatic bodies under uniform loading. However, for short and thick beams or plates, neither plane-stress nor plane-strain fully captures the three-dimensional stress state. Therefore, although plane-strain analysis could serve as an intermediate approximation for certain geometries and boundary conditions, a full three-dimensional elasticity formulation is generally required to

accurately represent the stress and deformation fields when the aspect ratio falls below unity.

Practical Implications. The accurate deflection formulas derived in this study have direct relevance for the design and analysis of structural components where high stiffness and minimal deformation are critical. Specifically, clamped beams are frequently encountered in precision mechanical systems, aerospace structures, Microelectromechanical Systems (MEMS), and fixed-end supports in civil and mechanical frameworks. In such applications, even small deflection inaccuracies can lead to performance degradation, misalignment, or fatigue-related failures. Therefore, the improved accuracy provided by the present finite element results offers a more reliable basis for structural optimization, tolerance evaluation, and safety assessment in advanced engineering designs.

Influence of Boundary Conditions and Boundary Layer Effects. The inability of classical analytical solutions—such as those proposed by Timoshenko, Roark, and Livesley—to accurately capture the physical response observed in numerical FEM results is primarily attributed to boundary layer phenomena that develop near clamped edges. These boundary layers are characterized by steep stress gradients and traction discontinuities, which cannot be fully represented by the smooth polynomial expressions inherent in closed-form solutions.

In the present FEM implementation, fully clamped boundary conditions were modeled by enforcing zero displacements in both transverse and in-plane directions along the fixed edges. This standard approach is generally sufficient for capturing the global deflection behavior within the studied aspect ratio range. However, the localized accuracy of stress fields near the supports remains sensitive to the precise manner in which these constraints are imposed. For instance, alternative treatments—such as introducing elastic restraints, applying penalty-based constraint enforcement, or refining the mesh in the vicinity of the supports—may influence both convergence behavior and the fidelity of boundary layer resolution.

Although a detailed parametric study on the effect of boundary condition implementation strategies is beyond the scope of this work, it represents an important avenue for future research. This is particularly relevant for applications demanding high fidelity in localized stress predictions, such as in fatigue-sensitive or failure-critical regions.

On the Shear Correction Factor and Its Broader Implications. The validation of shear correction factor introduced in this study emerges naturally from the comparison between detailed FEM results and classical beam theories, particularly those of Timoshenko and Roark. In the context of clamped beams under uniform transverse loading, it serves as a bridge between simplified analytical models and high-fidelity numerical simulations, correcting for discrepancies due to shear deformation effects. However, this factor is inherently problem-dependent, influenced by geometry, boundary conditions, and loading type. While the present work confines its analysis to a specific beam configuration, the underlying methodology—deriving correction factors from FEM benchmarking—can be extended to other

geometries (e.g., cantilevers, variable cross-section beams) and loadings (e.g., point loads, moments). A systematic investigation of such extensions could yield a more generalized framework for incorporating shear effects into simplified models, thereby enhancing their predictive accuracy across a broader class of structural problems.

While the Introduction addresses both displacement and stress analysis, this paper focuses solely on the former. Ongoing investigations into curve-fitting the normal stress along the clamp indicate that polynomial fitting is unsuitable. Instead, a high number of harmonics effectively captures its variation. A more detailed study of stress analysis and the corresponding shear-lag phenomenon [20]-[24] is planned for a subsequent publication.

9. Conclusion

This study demonstrates that the Finite Element Method (FEM) solution for a clamped beam subjected to a tip load is effectively bounded by three established closed-form analytical solutions: one providing a lower bound and two serving as upper bounds. However, a single correction factor cannot reconcile these analytical expressions with the FEM results due to the differing slopes of their respective linear regressions. To address this, we proposed fitted analytical expressions for four discrete Poisson's ratios, enabling estimation of maximum deflection as a function of aspect ratio within the range of 1 to 5. Additionally, we provided an algorithm and its source code for the general case of arbitrary Poisson's ratios ($\nu \in [0.15, 0.30]$) and aspect ratios ($\lambda \in [1, 5]$), offering a practical tool for comprehensive deflection analysis.

Conflicts of Interest

The author declares no conflicts of interest regarding the publication of this paper.

References

[1] Elishakoff, I. (2019) Who Developed the So-Called Timoshenko Beam Theory? *Mathematics and Mechanics of Solids*, **25**, 97-116. https://doi.org/10.1177/1081286519856931

[2] Timoshenko, S.P. (1921) LXVI. *On the Correction for Shear of the Differential Equation for Transverse Vibrations of Prismatic Bars. The London, Edinburgh, and Dublin Philosophical Magazine and Journal of Science*, **41**, 744-746. https://doi.org/10.1080/14786442108636264

[3] Timoshenko, S.P. (1922) X. *On the Transverse Vibrations of Bars of Uniform Cross-section. The London, Edinburgh, and Dublin Philosophical Magazine and Journal of Science*, **43**, 125-131. https://doi.org/10.1080/14786442208633855

[4] Xia, G. (2022) Generalized Foundation Timoshenko Beam and Its Calculating Methods. *Archive of Applied Mechanics*, **92**, 1015-1036. https://doi.org/10.1007/s00419-021-02090-1

[5] Öchsner, A. (2021) Classical Beam Theories of Structural Mechanics. Springer. https://doi.org/10.1007/978-3-030-76035-9

[6] Conway, H.D., Chow, L. and Morgan, G.W. (1951) Analysis of Deep Beams. *Journal of Applied Mechanics*, **18**, 163-172. https://doi.org/10.1115/1.4010271

[7] Chow, L., Conway, H.D. and Winter, G. (1953) Stresses in Deep Beams. *Transactions of the American Society of Civil Engineers*, **118**, 686-702. https://doi.org/10.1061/taceat.0006784

[8] Theocaris, P.S. (1959) The Stress Distribution in a Semi-Infinite Strip Subjected to a Concentrated Load. *Journal of Applied Mechanics*, **26**, 401-406. https://doi.org/10.1115/1.4012052

[9] Theocaris, P.S. (1964) The Method of Isostatics Applied to Rectangular Bars with Uniform Loading. *International Journal of Engineering Science*, **2**, 1-19. https://doi.org/10.1016/0020-7225(64)90007-2

[10] Benthem, J.P. (1963) A Laplace Transform Method for the Solution of Semi-Infinite and Finite Strip Problems in Stress Analysis. *The Quarterly Journal of Mechanics and Applied Mathematics*, **16**, 413-429. https://doi.org/10.1093/qjmam/16.4.413

[11] Horvay, G. and Born, J.S. (1957) Some Mixed Boundary-Value Problems of the Semi-Infinite Strip. *Journal of Applied Mechanics*, **24**, 261-268. https://doi.org/10.1115/1.4011507

[12] Johnson, M.W. and Little, R.W. (1965) The Semi-Infinite Elastic Strip. *Quarterly of Applied Mathematics*, **22**, 335-344. https://doi.org/10.1090/qam/187479

[13] Cowper, G.R. (1966) The Shear Coefficient in Timoshenko's Beam Theory. *Journal of Applied Mechanics*, **33**, 335-340. https://doi.org/10.1115/1.3625046

[14] Labuschagne, A., van Rensburg, N.F.J. and van der Merwe, A.J. (2009) Comparison of Linear Beam Theories. *Mathematical and Computer Modelling*, **49**, 20-30. https://doi.org/10.1016/j.mcm.2008.06.006

[15] Levinson, M. (1981) A New Rectangular Beam Theory. *Journal of Sound and Vibration*, **74**, 81-87. https://doi.org/10.1016/0022-460x(81)90493-4

[16] Timoshenko, S. and Goodier, J.N. (1970) Theory of Elasticity. 3rd Edition, McGraw-Hill, 46.

[17] Augarde, C.E. and Deeks, A.J. (2008) The Use of Timoshenko's Exact Solution for a Cantilever Beam in Adaptive Analysis. *Finite Elements in Analysis and Design*, **44**, 595-601. https://doi.org/10.1016/j.finel.2008.01.010

[18] Livesley, R.K. (1983) Finite Elements: An Introduction for Engineers. Cambridge University Press, 94-95.

[19] Young, W.C. (1989) Roark's Formulas for Stress & Strain. 6th Edition, McGraw-Hill, 201-202.

[20] Argyris, J.H. (1954) Diffusion of Antisymmetrical Loads into, and Bending under, Transverse Loads of Parallel Stiffened Panels, Reports & Memoranda No. 2822 (9662), A.R.C. Report. https://www.abbottaerospace.com/downloads/arc-rm-2822-diffusion-of-antisymmetrical-loads-into-and-bending-under-transverse-loads-of-parallel-stiffened-panels/

[21] Megson, T.H.G. (1990) Aircraft Structures for Engineering Students. 2nd Edition, Adward Arnold.

[22] Hadji-Argyris, J. and Dunne, P.C. (1949) The General Theory of Cylindrical and Conical Tubes under Torsion and Bending Loads. *The Journal of the Royal Aeronautical Society*, **53**, 558-620. https://doi.org/10.1017/s0368393100120188

[23] Reissner, E. (1946) Analysis of Shear Lag in Box Beams by the Principle of Minimum Potential Energy. *Quarterly of Applied Mathematics*, **4**, 268-278.

https://doi.org/10.1090/qam/17176

[24] Chang, S.T. and Zheng, F.Z. (1987) Negative Shear Lag in Cantilever Box Girder with Constant Depth. *Journal of Structural Engineering*, **113**, 20-35. https://doi.org/10.1061/(asce)0733-9445(1987)113:1(20)

Appendix

Below, we provide the MATLAB® (ver. R2014) computer code that calculates the maximum shear displacement V_s of a clamped beam, of given elastic modulus $E=1$ and tip-load $P=1$, as illustrated in **Figure 1**. The true parameters of this program are the aspect ratio $\lambda = L/h$ (variable lambda) and Poisson's ratio ν (variable nu). The calculation is based on tedious FEM results, which have been stored in vectors.

The structure of the code is as follows:

Xvector: Discrete values of aspect ratios λ for which FEM was conducted.

Yvector15: The corresponding FEM-based maximum shear deflection for $\nu = 0.15$.

Yvector20: The corresponding FEM-based maximum shear deflection for $\nu = 0.20$.

Yvector25: The corresponding FEM-based maximum shear deflection for $\nu = 0.25$.

Yvector30: The corresponding FEM-based maximum shear deflection for $\nu = 0.30$.

```
%*****************************************************************
% CALCULATION OF MAXIMUM SHEAR DISPLACEMENT FOR A CLAMPED BEAM %
%*****************************************************************
clear all; clc;
%-------------------------------------------------------------------------
%% DATA:
lambda = 3.0;   %DATA (aspect ratio)
xnu    = 0.20;  %DATA (Poisson's ratio)
%-------------------------------------------------------------------------
Xvector=[1.0 1.5 2.0 2.5 3.0 3.5 4.0 4.5 5.0];  %Stored Aspect Ratios
XNU_vector=[0.15 0.20 0.25 0.30];               %Stored Poisson's ratios
%-------------------------------------------------------------------------
%% FEM results (Shear deflecton) stored in following vectors:
%% Poisson's ratio xnu=0.15;
Yvector15=[2.676262411257414   4.021809648247569   5.358504189437880  ...
6.686321234870697   8.005037363892399   9.314331970398570  ...
10.613747159425827  11.902739986980976  13.180519494768816];
%% Poisson's ratio xnu=0.20;
Yvector20=[2.774365078728927   4.159939475015129   5.530187872399281   ...
6.885109870785819   8.224460551646800   9.547899291536083   ...
10.854935378930804  12.145018848933660  13.417298787103448];
%% Poisson's ratio xnu=0.25;
Yvector25=[2.869506424472671   4.291196764702800   5.689446178845692   ...
7.064268936127043   8.415387917331998   9.742430923993481  ...
11.044855949928603  12.322098545149572  13.573206121168653];
%% Poisson's ratio xnu=0.30;
Yvector30=[2.961818588899186   4.415883096106974   5.836817412815648   ...
7.224639785307140   8.579029199727003   9.899568440265767  ...
11.185645855631606  12.436666554785461  13.651548593491555];
%% LINEAR INTERPOLATION based on the given Aspect ratio:
%---Interpolate on the four polygonal lines of FEM-results:
Y15=interp1(Xvector,Yvector15,lambda);%interpolate on curve xnu=0.15
Y20=interp1(Xvector,Yvector20,lambda);%interpolate on curve xnu=0.20
Y25=interp1(Xvector,Yvector25,lambda);%interpolate on curve xnu=0.25
Y30=interp1(Xvector,Yvector30,lambda);%interpolate on curve xnu=0.30
%---Store the finding for all the four Poisson's ratios:
Ysequence = [Y15 Y20 Y25 Y30];  %store all four Vs-values
%---Linear interpolate for the given Poisson;s rtio:
disp('*** LINEAR INTERPOLATION ***')
Vs=interp1(XNU_vector,Ysequence,xnu);   %linear interplate for given xnu.
disp(['Maximum Shear Deflection Vs-max = ', num2str(Vs)]);
return
```